Applied Science and Innovative Research
ISSN 2474-4972 (Print) ISSN 2474-4980 (Online)
Vol. 9, No. 1, 2025
www.scholink.org/ojs/index.php/asir

*Original Paper*

# Satellite Remote Sensing Estimation of Ground Subsidence along Transmission and Transformation Lines Based on Multi-scale Geographically Weighted Regression

Xiao Li[1], Qingkun Yang[1], Chen Cao[1], Tie Jin[1] & Xiguan An[1]

[1] College of Construction Engineering, Jilin University, Changchun 130012, Jilin, China

Received: January 20, 2025 Accepted: February 22, 2025 Online Published: February 28, 2025

doi:10.22158/asir.v9n1p146 URL: http://doi.org/10.22158/asir.v9n1p146

***Abstract***

*In this paper, a 5km area along the 750kV Third passage project in Shaanxi Province is taken as the research area. Based on the analysis of the application and limitation of traditional two-dimensional regression model in land subsidence simulation, the advantages of multi-scale geographical weighted regression model in automatically calculating bandwidth and exploring spatial heterogeneity of impact factors are explored. Based on the geological environment of the region and the latest geological disaster data, seven influencing factors including slope, topographic relief, average annual rainfall, topographic humidity index (TWI), distance from river, distance from fault and distance from road were selected as dependent variables, and the SBAS-InSAR results covering the whole region were taken as independent variables. On the basis of evaluation factor analysis, The land subsidence results along the 750kV third passage project in northern Shaanxi and Guanzhong were simulated by ArcGIS platform. The evaluation results show that the fault distance and precipitation in the study area have great influence.*

***Keywords***

*Land subsidence multi-scale geographical weighted regression InSAR driving force analysis*

## 1. Introduction

As the social electricity consumption in Shaanxi Province increases year by year, it is of great importance to improve the intelligent level of power grid, support cross-regional power trading and rural electrification, and ensure the safe construction and operation of line projects (Xie Huafei, 2011). Transmission lines have the characteristics of long distance and long span. At the same time, due to the complex and fragile engineering geological conditions, the monitoring of geological hazards in the transmission line area is particularly heavy (Liu Hujun, 2004). The main part of Shaanbei - Guanzhong

750kV third channel project is located in Weinan City, the east of Weihe Basin and the southern margin of the Loess Plateau. It has complex geological structure, large topographic relief and active fault movement (He Hongqian, 2011; Zhao Jingbo & Chen Yun, 1994). Loess is the main type of soil in the region, which has the characteristics of large porosity and high water content, and is prone to compression and settlement when the water content changes caused by external forces or rainfall factors (Zhang Maosheng & Li Tonglu, 2011; Zhang Puxuan, 2017). The groundwater resources in the study area are abundant. In the process of engineering construction or agricultural irrigation, a large amount of groundwater will be extracted, which will easily lead to ground settlement and subsidence funnel, threatening the stability of transmission line base (Yin Yueping, Zhang Zuochen, & Zhang Kaijun, 2005). Land subsidence is a kind of slow regional geological disaster caused by groundwater, mineral resource exploitation, crustal movement and other factors (F. Raspini, F. Caleca, M. Del Soldato, D. Festa, P. Confuorto, S. Bianchini, 2022). At present, in the study of land subsidence, in addition to the use of high-precision geometric leveling, telescopometer, global navigation satellite system or global positioning system network to detect it, satellite remote sensing means, especially synthetic aperture radar interferometry technology, are also used to study land subsidence (Fan Shan-Shan, Guo Hai-Peng, Zhu Ju-Yan, et al., 2013), and its effectiveness in this field has been repeatedly proved. 0Compared with the original methods, InSAR technology has great advantages in monitoring scope and monitoring cost, and is less affected by climate. The millimeter-level accuracy, wide area data coverage, high frequency data sampling, ability to track deformation history, and higher benefit/cost ratio compared to targeted ground monitoring activities have led to the increasing use of SAR interferometry in the field of land subsidence research.

In order to predict land subsidence, and then plan and guide the key areas of deformation in the construction and operation of transmission lines, researchers choose to use regression analysis method to quantify the influence of variables and analyze the causal relationship between multiple independent variables (Li Li, 2014; Li Guangyu, Zhang Rui, Liu Guoxiang, et al., 2018; Xiong Q., 2023). Ordinary least squares (OLS) is the simplest regression analysis method, which can directly explain the average influence of each variable on the dependent variable. However, if the land subsidence in different regions is significantly affected by different factors, the OLS hypothesis is no longer applicable. On this basis, the consideration of spatial heterogeneity and optimal bandwidth is added, and a geographically weighted regression model (GWR) and a multi-scale geographically weighted regression model (MGWR) are gradually produced, among which the fitting error of the MGWR model is significantly smaller than that of GWR and OLS. Huang Shuangfei (2024) took Qingchuan County, Guangyuan City, Sichuan Province as the research object, and selected elevation, slope, slope direction, relief of terrain, rock, rainfall, distance from fault zone, distance from water system, distance from residential site, and vegetation cover type as independent variables to study landslide susceptibility. The results show that MGWR model can realize factor correlation and spatial non-stationary integration. Previous studies have shown that the reasonable use of multi-scale geographical weighted regression model can improve the accuracy of regional land subsidence simulation.

By allowing independent variables to function on different spatial scales, MGWR model structure is more flexible, and the most suitable spatial scale can be selected for different independent variables, thus improving the adaptability and flexibility of the model. It can more accurately reflect the influence of each independent variable in different regions, and improve the explanatory power and accuracy of the model; More local details and changes can be captured to better reflect complex spatial structures and relationships; Better adapt to the spatial changes of data, improve the fit degree and prediction accuracy of the model. This paper adopts the multi-scale geographical weighted regression method; The influence of different independent variables on different spatial scales, so as to improve the reliability and accuracy of ground settlement prediction of transmission lines. This study conducted field geological survey on route selection, combined with geotechnical investigation data in the region, and selected 7 independent variables including slope, topographic humidity index, distance from river, distance from road, distance from fault, average annual rainfall and topographic relief. Based on single-scale geographical regression analysis model and MGWR model, ArcGIS platform was adopted to analyze the results. The ground subsidence rate of transmission and transformation line selection was simulated to verify the accuracy of the simulation results, and the simulation results were compared in order to better understand the relationship between ground subsidence and its influencing factors, and at the same time to provide certain basis for line selection, power tower site selection and subsequent safe operation.

## 2. Overview of the Research Area

The main part of the Shaanbei - Guanzhong 750kV third passage project is located in Weinan City, Shaanxi Province, in the east of Weihe Basin. The geographical coordinates are 34°15'20.42"~35°25'22.02" N, 109°26'29.56"~109°49'06.96" E, and the research area is 5km on both sides of the route. The length of the line is 2×161km, and the research area is 883.54km$^2$.

The northern section of the line is located on the edge of the Ordos block and in the transition area between the basin and the Loess Plateau. The middle section is located in the eastern section of Weihe Cenozoic faulted basin in Guanzhong Basin; The southern section is adjacent to the Qinling Mountains, which is the Qinling fold transition zone of the Weihe fault depression basin (Li Xianggen & Ran Yongkang, 1983). A series of active faults (Feng Xijie & Dai Wangqiang, 2004; Peng Jianbing, Su Shengrui, & Mi Fengshou, 1992) developed in and along the margin of the Weihe fault Basin, an area with frequent neotectonic activity along the line, which is manifested by large differences in block uplift and subsidence and frequent seismic activity at the junction of uplift and fault depression (Quan Xinchang, 2005; Peng Jianbing et al., 2012; Yue-fei Wang, 2023). The landforms are distributed in a banding pattern, from south to north, the landforms are successively mountainous, alluvial plain, alluvial plain, loess tableland and mountainous area. The thickest part of the Quaternary system is over 700m, which is located in the north of Linwei Area (Daniel Yuh Chao, 2019). The terrain is high in the north and south and low in the middle, with an elevation ranging from 340.0m to 1100.0m (S. Ye, Y. Xue, J. Wu, X.

Yan, & J. Yu, 2015). The study area belongs to the temperate semi-arid continental monsoon climate, with strong spatio-temporal difference of rainfall, which is concentrated in summer, and its spatial distribution is more in the north and south, less in the middle. Weihe River and Beiluo River are the most developed rivers in this region.

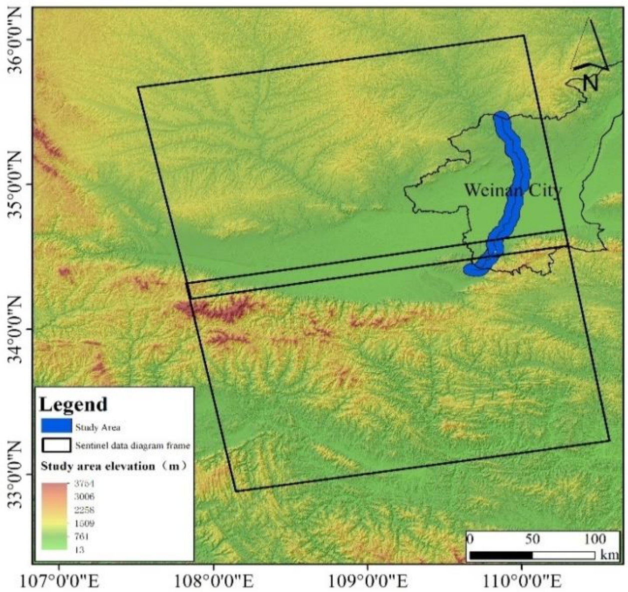


**Figure 1. Overview Map of the Study Area**

## 3. Study Method

### *3.1 SBAS-InSAR Technique*

Small-baseline synthetic aperture radar interferometry (SBAS-InSAR) solves the problem of incoherence caused by too long spatial baseline of conventional InSAR technology, which can fully improve the resolution of data sampling time, monitor large areas and non-urban areas, and use the settled displacement rate and accumulated displacement as the ground settlement number (P. Berardino, G. Fornaro, R. Lanari, & E. Sansosti, 2002).

The principle of SBAS-InSAR technology is as follows: suppose that N+1 radar data images are acquired in the study area within the time period of $t_{N0}$~t, and certain time and space thresholds are set for them. After interference processing, M-amplitude differential interferography is obtained (H. Yu, A.S. Fotheringham, Z. Li, T. Oshan, W. Kang, L.J. Wolf, 2020). M satisfies the equation as follows:

$$\frac{N+1}{2} < M < \frac{N(N+1)}{2} \tag{1}$$

For$_A$ the phase j interfero$_B$gram obtained from the main image and generated from the image at two time points $t_B$ and t ($t_A$<t), the interference phase of any point in the diagram is:$(x, r)$

$$\delta\phi_j(x,r) = \phi(t_B, x, r) - \phi(t_A, x, r) \approx \Delta\phi_{disp} + \Delta\phi_{topo} + \Delta\phi_{orb} + \Delta\phi_{atm} + \Delta\phi_{noise} \tag{2}$$

In Formula 3-8, and represents the phase of the two images at the point; $\phi(t_B, x, r)\phi(t_A, x, r)(x, r)\Delta\phi_{disp}$ Is the cumulative deformation of$_{AB}$ the object along the line of sight of the satellite at time $t_0$ and t relative to t; $\Delta\phi_{topo}, \Delta\phi_{orb}, \Delta\phi_{atmo,}\Delta\phi_{noise}$ Refers to the phase errors caused by terrain, orbit, atmosphere and noise respectively.

When the deformation error caused by the atmosphere, noise, terrain and track is removed, the phase change can be expressed as:

$$\delta\phi_j(x,r) = \phi(t_B,x,r) - \phi(t_A,x,r) \approx \frac{4\pi}{\lambda}[d(t_B,x,r) - d(t_A,x,r)] \tag{3}$$

In formula (9), represents deformation. $d\ (t_A,x,r)d\ (t_B,x,r)$. Let the initial time deformation be 0, then the phase time series of the interferogram is:

$$\phi(t_i,x,r) = \frac{4\pi}{\lambda}d(t_i,x,r)(i = 1,\ldots,N) \tag{4}$$

A point variable represented by a vector is:

$$\phi = [\phi(t_1),\ldots,\phi(t_N)]^x \tag{5}$$

Then the vector composed of the interferogram phase, whose value is:

$$\delta\phi = [\delta\phi_1,\ldots,\delta\phi_M]^x \tag{6}$$

$\delta\phi_i(i = 1,\ldots M)$ Is the phase value of each point relative to the reference point. For the master and slave images, the phase value can be expressed as:

$$\delta\phi = A\phi \tag{7}$$

A is a matrix of MN, where each row corresponds to an interference relative. ×When the phase solution is converted to the problem of the rate of phase change, equation (7) can be converted to:

$$Bv = \delta\phi \tag{8}$$

In the formula, B is MN matrix, SVD processing of the matrix, the average velocity v can be obtained, and then the integral operation can solve the deformation information of each pixel of the interferogram.×

*3.3 K-means Cluster Analysis*

The K-Means method divides the data into several uniform clusters with similar features, initializes the center of the k-cluster with a random search in each iteration, and then measures the distance from the data point ($X_{ij}$) to the center ($C_j$). The cluster k is assigned to the data point $x_{ij}$ by minimizing the objective function specified by formula (9). Due to the large study area and large amount of InSAR deformation data, in order to shorten the calculation time of the model while preserving the data properties, the clustering analysis method is adopted.

*3.3 Single Scale Two-dimensional Regression Model*

The OLS model establishes the relationship between the dependent variable and one or more independent variables on a global scale by means of least square method. This relationship is also known as classical linear regression, and its equations are:

$$y_i = \beta_0 + \sum_{k=1}^{m}\beta_k x_{ik} + \varepsilon_i \tag{9}$$

Geographically weighted regression model (GWR model) is the regression coefficient of independent variables in the model changes at different local points, so as to contain local variation, which can depict a more accurate relationship between variables in the data, and calculate the local independent variable coefficient by weighted least square method in the form of independent matrix (H. Yu, H. Gong, B. Chen, K. Liu, M. Gao, 2020; L. Zhang, Y. Li, R. Li, 2023):

$$\hat{\beta}_{ik} = [X^T W_i X]^{-1} X^T W_i Y \tag{10}$$

Its equation is as follows:

$$y_i = \beta_0(u_i, v_i) + \sum_{k=1}^{m} \beta_k(u_i, v_i) x_{ik} + \varepsilon_i \tag{11}$$

*3.4 Multi-scale Geographical Weighted Regression Model*

To better understand the drivers behind land subsidence, regression analysis of SBAS-InSAR results can be performed using machine learning methods. Combined with the land subsidence impact factor data, a land subsidence prediction model can be built. The ordinary least squares (OLS) method is the most basic global method in regression analysis, but it does not consider the scale factor. The GWR method solves the scaling problem by calculating the optimal bandwidth, taking into account the spatial heterogeneity to a certain extent, but each of its influencing factors is limited to the same scale. To overcome this limitation, the MGWR method allows to examine spatial heterogeneity by relaxing different influencing factors at different scales (A.S. Fotheringham, W. Yang, W. Kang, 2017). Its equation is as follows:

$$y_i = \beta_{bwo}(u_i, v_i) + \sum_{k=1}^{m} \beta_{bwk}(u_i, v_i) x_{ik} + \varepsilon_i \tag{12}$$

Where: is the longitude and latitude of the space position i. $(u_i, v_i)\beta_{bwo}(u_i, v_i)$ Is the constant term, is the local coefficient estimate of the KTH independent variable; $\beta_{bwk}(u_i, v_i)y_i$, m and are the same parameters as MGWR.$x_{ik}\varepsilon_i$

*3.5 Model Accuracy Verification Method*

The use of post-fit algorithms during calibration allows for iterative estimates of additive terms, which can improve the accuracy of the model. To capture the nonlinear relationship between the dependent and independent variables, the model should be converted to a generalized additive model form, as shown in the equation:

$$\hat{y} = \sum_{k=1}^{m} \widehat{f_k} + \hat{\varepsilon} \tag{13}$$

The convergence termination criterion is determined by the rate of change of the sum of squares of residuals (SOCRSS). The change in fraction between successive iterations can be expressed as follows:

$$SOC_{RSS} = \left| \frac{RSS_2 - RSS_1}{RSS_2} \right| \tag{14}$$

In the SM-GWR method, the spatial weight matrix is determined based on the 3D spatial distance between the calibration position and the adjacent position. The closer the adjacent position is to the calibration position, the stronger its effect. The double quadratic kernel function is used to calculate the spatial weight matrix, focusing only on the influence of nearby points on the bandwidth determination, and its formula is as follows:

$$w_{ij} = \begin{cases} \left[1 - \left(\frac{d_{ij}}{b}\right)^2\right]^2, if \left|d_{ij}\right| < b \\ 0, otherwise \end{cases} \tag{15}$$

Where an indicator of the Euclidean distance separating the local calibration point i from its corresponding observation point j; $d_{ij}$b represents the bandwidth parameter. This weight decreases as the distance between the two observations increases, and more if the distance is closer to the bandwidth parameter. If the distance between the two observations is greater than the bandwidth parameter, the weight is set to zero.

Bandwidth selection is usually performed using modified Akaike Information Criteria (AICc). This standard prevents the selection of smaller bandwidths, which can complicate the model. Therefore, this helps prevent overfitting and non-smooth fitting. The calculation formula used to select the optimal bandwidth for the AICc represents the following formula:

$$AIC_c = 2n \log_e \left(\frac{RSS}{n}\right) + n \log_e 2\pi + n \left\{\frac{n+tr(S)}{n-2-tr(S)}\right\} \tag{16}$$

Lower AICc and RSS values indicate an improved level of reproducibility of the independent variable. RSS is used to evaluate model accuracy

$$RSS = \sum_{i=1}^{n} \left(y_{pred,i} - y_{obs,i}\right)^2 \tag{17}$$

$R^2$ is used to evaluate the fit of the model (Hu, B., Zhou, J., Wang, J., Chen, Z., Wang, D., & Xu, S., 2009)

$$R^2 = 1 - RSS/\sum_{i=1}^{n} \left(y_{obs,i} - \bar{y}_{obs}\right) \tag{18}$$

Where denotes the predicted value, denotes the actual value, and denotes the average true value. $y_{pred} y_{obs} \bar{y}_{obs}$

T-value tests are used as partial tests to evaluate a model, and by validating individual parameter estimates, potential errors or inaccuracies in the model can be identified, and necessary adjustments can then be made.

$$t_{(i,j)} = \frac{\hat{\beta}_{(i,j)}}{se_{(i,j)}} \tag{19}$$

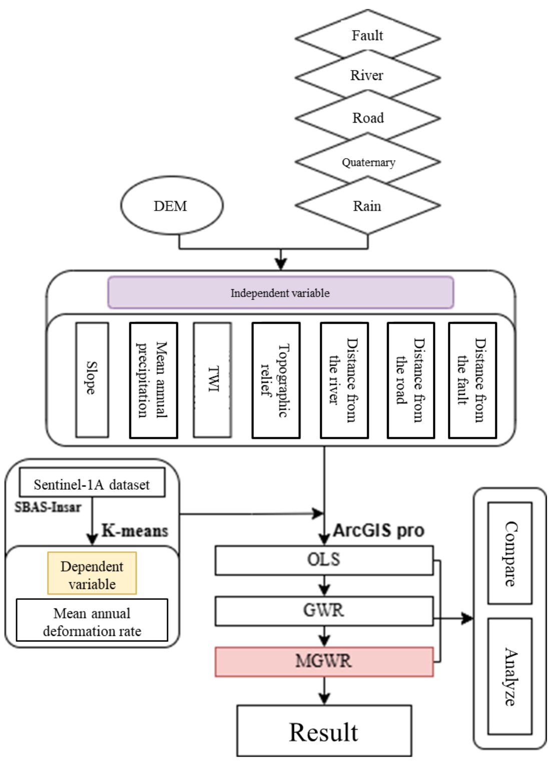


**Figure 2. Technology Roadmapping**

## 4. Data Processing

### *4.1 InSAR Data Processing*

In this paper, Sentinel-1A satellite is used to obtain synthetic aperture radar images of the study area, and 70 scenes of descent orbit data are selected for processing. The oblique range resolution is 13.93 meters, and the image time is five years from February 4, 2018 to May 21, 2023. The polarization mode is VV polarization and the incidence Angle is 39.60 °. In addition, the distance resolution is 2.33 meters and the azimuth syncline distance resolution is 14.01 meters. Table 1 presents the radar data series for the study area.

**Table 1. Sentinel-1A SAR Dataset**

| Sn. | Image time | Serial number | Image time | Serial number | Image time | Serial number | Image time |
|---|---|---|---|---|---|---|---|
| **1** | 20180204 | **21** | 20190530 | **41** | 20201015 | **61** | 20220502 |
| **2** | 20180216 | **22** | 20190623 | **42** | 20201108 | **62** | 20220526 |
| **3** | 20180312 | **23** | 20190717 | **43** | 20201226 | **63** | 20220806 |
| **4** | 20180405 | **24** | 20190810 | **44** | 20210119 | **64** | 20221204 |
| **5** | 20180429 | **25** | 20190927 | **45** | 20210212 | **65** | 20221228 |
| **6** | 20180523 | **26** | 20191021 | **46** | 20210401 | **66** | 20230121 |
| **7** | 20180616 | **27** | 20191114 | **47** | 20210425 | **67** | 20230226 |
| **8** | 20180710 | **28** | 20191208 | **48** | 20210519 | **68** | 20230322 |
| **9** | 20180803 | **29** | 20200101 | **49** | 20210706 | **69** | 20230427 |
| **10** | 20180827 | **30** | 20200125 | **50** | 20210811 | **70** | 20230521 |
| **11** | 20180920 | **31** | 20200218 | **51** | 20210904 | | |
| **12** | 20181014 | **32** | 20200313 | **52** | 20210928 | | |
| **13** | 20181107 | **33** | 20200406 | **53** | 20211022 | | |
| **14** | 20181201 | **34** | 20200430 | **54** | 20211115 | | |
| **15** | 20181225 | **35** | 20200524 | **55** | 20211209 | | |
| **16** | 20190118 | **36** | 20200617 | **56** | 20220102 | | |
| **17** | 20190211 | **37** | 20200711 | **57** | 20220126 | | |
| **18** | 20190319 | **38** | 20200804 | **58** | 20220219 | | |
| **19** | 20190412 | **39** | 20200828 | **59** | 20220315 | | |
| **20** | 20190506 | **40** | 20200921 | **60** | 20220408 | | |

The results show that the overall average deformation rate during the monitoring period is -19.19 ~ 6.42 mm/y, and the whole study area presents uneven subsidence. The main subsidence areas exist in Linwei District, Pucheng County and Chengcheng County, and a relatively obvious continuous subsidence phenomenon is formed, which has a wide influence area and a large subsidence rate, and the subsidence area is about 600 $km^2$. In Linwei District, the surface uplift and subsidence existed simultaneously. The largest subsidence area is located in Tangshan Bay Ecological City.

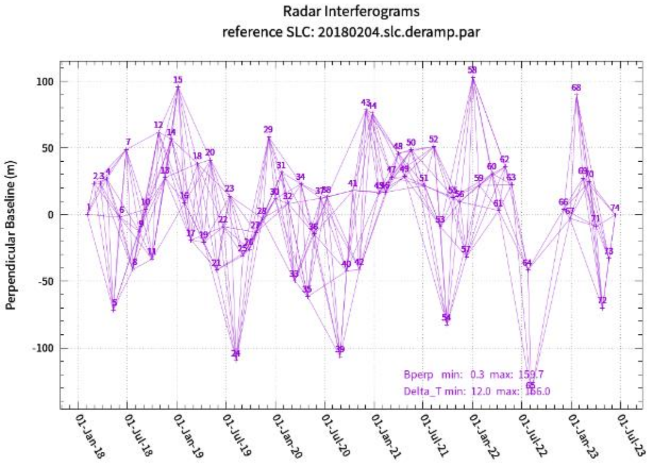


**Figure 3. Technology Roadmapping**

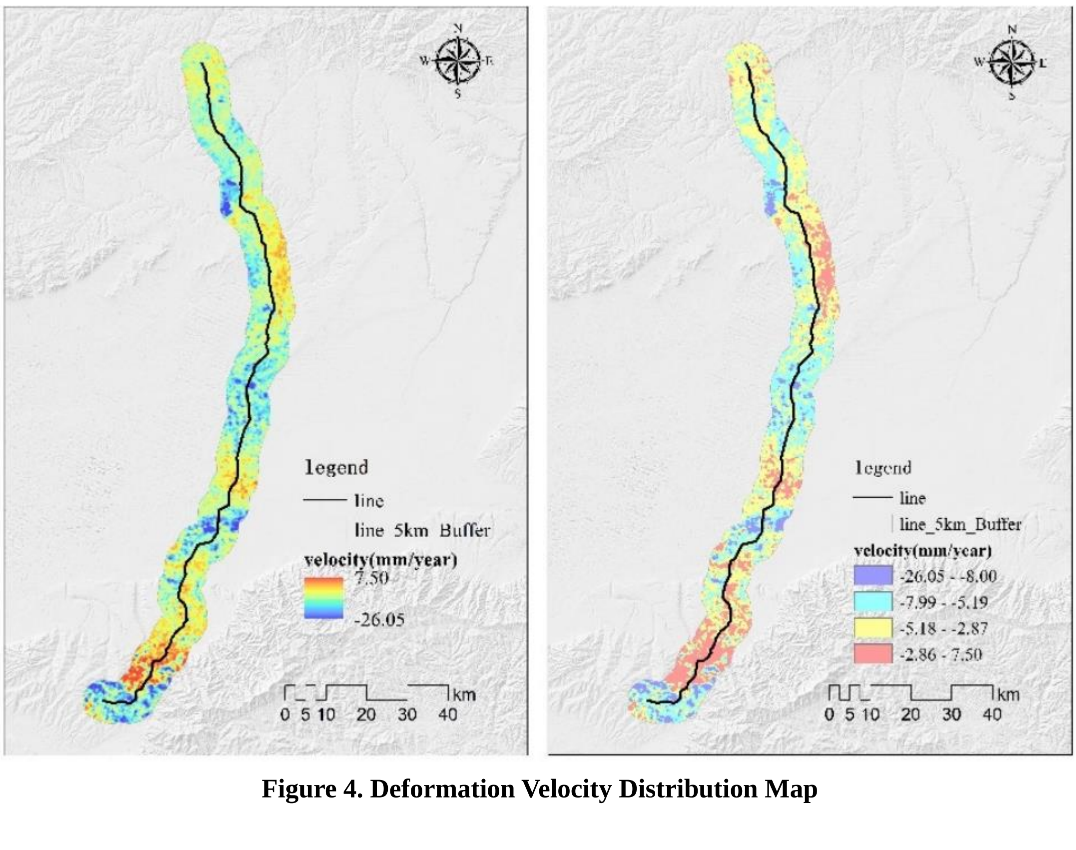


**Figure 4. Deformation Velocity Distribution Map**

*4.2 Selection and Analysis of Independent Variables*

4.2.1 Slope

Slope plays a strong controlling role in the development and occurrence of geological hazards, and determines the stress state and stability of slope. At the same time, slope also has an impact on surface runoff and groundwater (Wang Zhiwang, Liao Yonglong, & Li Duanyou, 2006). In order to consider the impact of slope on geological hazards in the study area, a slope grid map was obtained based on the digital elevation model (DEM) of the study area and the slope analysis function of ArcGIS platform. According to the natural breakpoint classification method by ArcGIS platform, they were classified into 5 categories: 0~4.24°, 4.24°~9.55°, 9.55°~16.98°, 16.98°~26.80° and 27.80°~67.66° (Figure 4a).

#### 4.2.2 Topographic Relief

For the loess tableland and hilly landform contained in the study area (Zhao Wenwu, Fu Bojie, & Chen Liding, 2003), topographic relief is an important and typical influencing factor of land subsidence in the study area (Fadhillah, M.F., Achmad, A.R., & Lee, C., 2020). Topographic relief was calculated based on DEM in the study area, and it was divided into 5 groups, namely, 2-34, 34-69, 69-111, 111-179, and 179-399 (Figure 4b).

#### 4.2.3 Distance from River

In the study area, there are many rivers with different discharge, and some routes are selected near the riverbank and need to cross Luo River and other rivers repeatedly. According to the river vector data of the study area, six distance grade river buffers of 0~100m, 100~200m, 200~400m, 400~600m, 600~800m, 800~1000m and >1000m were established through the multi-ring buffer function of ArcGIS platform (Figure 4c).

#### 4.2.4 Distance from the Road

The traffic load on the road, especially the frequent passage of heavy vehicles, will have a dynamic effect on the soil growth period of the foundation near the road. This repeated load will lead to gradual compaction and deformation of the foundation soil, and eventually lead to ground settlement. The closer the area is to the road, the more obvious the impact of traffic loads (Wang, W., Wu, L., Gong, H., Fan, P., Wu, W., Zhou, Y., & Zhang, Z., 2019). By using the ArcGIS platform multi-ring buffer function, six distance levels of road buffer zones of 0~100m, 100~200m, 200~400m, 400~600m, 600~800m, 800~1000m and >1000m are established (Figure 4d).

#### 4.2.5 Distance from Fault

Geological structure is an important factor affecting the development of geological disasters. The rock mass in the complex structure area is broken, the weathering is serious, and the slope integrity is low. At the same time, precipitation seeps into the slope along the structural cracks, reducing the strength of the slope [34]. 0By using the ArcGIS platform's multi-ring buffer function, fault buffers were created, which were classified into 6 categories of 0~2000m, 2000~5000m, 5000~10000m, 10000~20000m, 20000~40000m and >40000m (Figure 4e).

#### 4.2.6 Topographic Humidity Index

Topography can affect the flow direction of groundwater and the secondary distribution of precipitation, thus affecting the spatial distribution of water and the strength of different rock and soil bodies on the surface. Therefore, topography has an important impact on the occurrence of land subsidence (Wang, J., Wang, C., Zhang, H., Tang, Y., Duan, W., & Dong, L., 2021). In order to study the impact of topography on land subsidence in the study area, topographic humidity index (TWI) is introduced to express the spatial distribution of water in rock and soil mass. The formula is as follows:

$$TWI = \ln \frac{\alpha}{\tan \beta}$$

Where: is the catchment area; $\alpha\beta$Is slope. According to the digital elevation model (DEM) of the study area and the raster calculator function of ArcGIS platform, the raster map of terrain wetness index is obtained. Based on the natural breakpoint function of ArcGIS platform, It was reclassified into 5 categories of 3.10~6.62, 6.62~8.29, 8.29~10.47, 10.47~13.73, 13.73~24.44 (Figure 4f). With the increase of TWI value, the density of geological hazard points showed a decreasing trend.

4.2.7 Average Annual Rainfall

Rainfall has a positive effect on land subsidence, and the occurrence of land subsidence usually has a strong correlation with rainfall in time. In this paper, the average annual rainfall from 2018 to 2023 is used as an independent variable, and the grid data of average annual precipitation in the study area is generated according to the obtained precipitation nc data, and based on the natural breakpoint function of ArcGIS platform. It was reclassified into 5 categories of 6268~6532, 6532~6831, 6831~7118, 7118~7336 and 7336~7732 (Figure 4g).

**Table 2. Characteristics of Independent Variables in the Study Area**

| Variables | Code | Range | Unit |
|---|---|---|---|
| Average annual settling rate | Y | -19.19-6.42 | mm/a |
| Slope | SLOPE | 0-67.44 | ° |
| Topographic relief | TER_UNDU | 2-399 | - |
| Distance from fault | FAULT_DIST | 0-4971.62 | m |
| Distance from road | ROAD_DIST | 0-723.90 | m |
| Rainfall | RAIN | 6268.6-7732.2 | mm |
| Topographic humidity index | TWI | 2.512-24.459 | - |
| Distance from river | RIVER_DIST | 0-20337.1 | m |

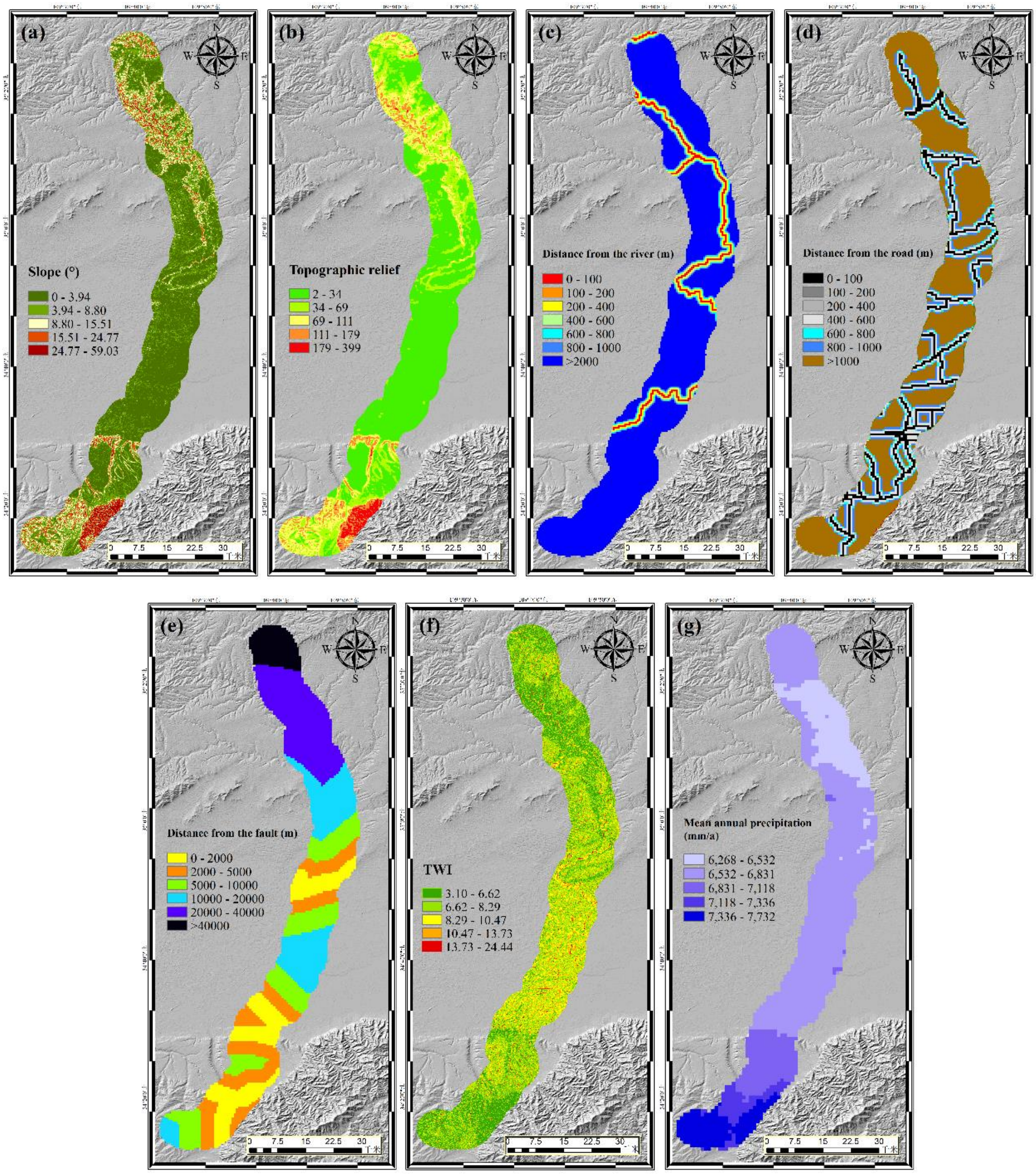


**Figure 4. Independent Variables of Classification**

a. Distribution Map of Slope; b. Distribution Map of Topographic Relief; c. Distribution Map of Distance from Rivers; d. Distribution Map of Distance from Roads; e. Distribution Map of Distance from Faults; f. Distribution Map of Topographic Wetness Index; g. Distribution Map of Annual Average Precipitation

The independent variables above were selected, and the annual deformation rate was taken as the dependent variable. The analysis was carried out through OLS, GWR and MGWR models, and the analysis results were compared respectively to obtain the most influential factors, and the accuracy of the three models in the analysis and calculation process was analyzed.

## 5. Model Results and Verification

### *5.1 Three Model Results*

5.1.1 Analysis of Simulation Results

GWR model and MGWR model were used to predict the deformation rate of the study area respectively, and the prediction results were shown in Figure 5. By comparing the distribution of the predicted deformation rate results with the calculated results of SBAS-InSAR, it can be seen that the predicted deformation distribution is consistent with the reality, and the average annual deformation rate calculated by the MGWR model ranges from -4.12-2.75mm/y. The average annual deformation rate calculated by the GWR model ranges from 0.319 to 0.859mm/y, and compared with the overall average deformation rate of -19.19 to 6.42 mm/y during the monitoring period, it can be seen that the prediction result of the MGWR model is more accurate.

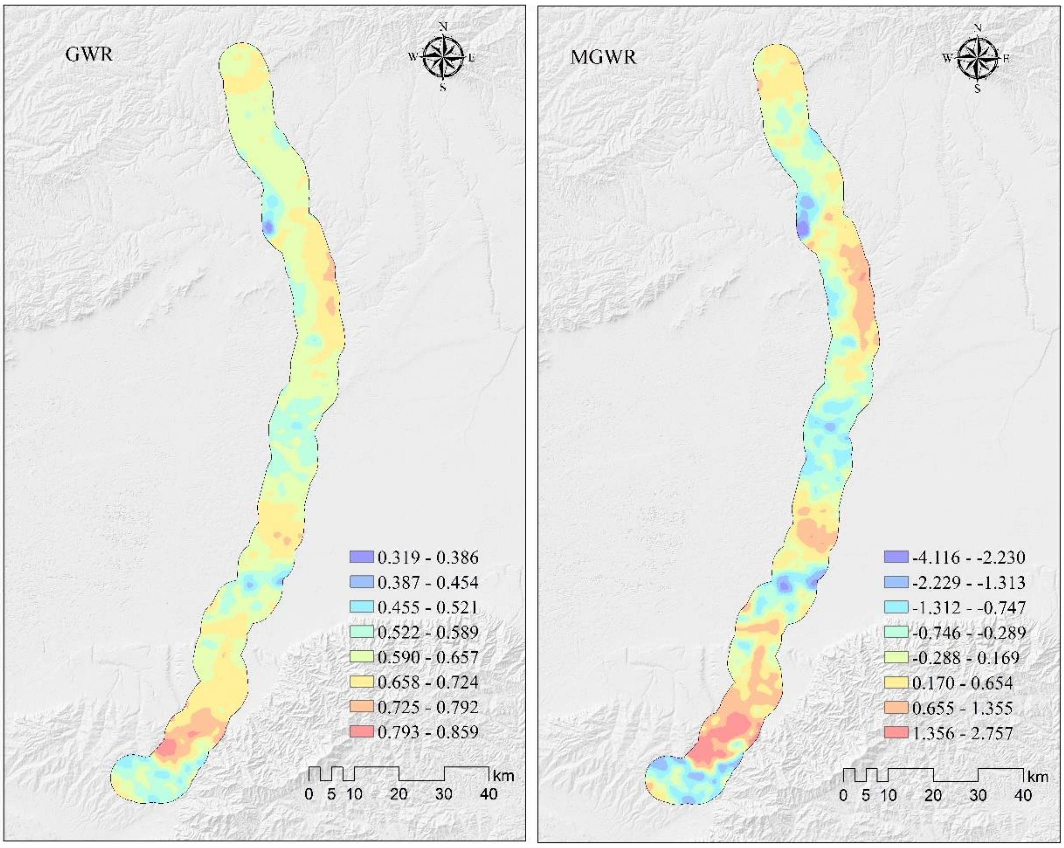


**Figure 5. Estimated Annual Average Subsidence Rate of the Study Area**

**Table 3. Performance Table of Independent Variables of the MGWR Model in the Study Area**

| Dependent variable | Average annual settling rate | | | | |
|---|---|---|---|---|---|
| Performance values | Average | Minimum | Maximum | T-value | Alpha value |
| Slope | 0.033 | -0.017 | 0.062 | 2.448 | 0.041 |
| Topographic relief | 0.087 | 0.048 | 0.167 | 2.364 | 0.044 |
| Distance from fault | -0.613 | -6.203 | 3.063 | 3.748 | 0.010 |
| Distance from road | 0.046 | -2.679 | 1.662 | 3.756 | 0.009 |
| Rainfall | -1.346 | -1.543 | -1.183 | 2.253 | 0.047 |
| Topographic humidity index | 0.004 | -0.049 | 0.039 | 2.545 | 0.038 |
| Distance from river | -0.324 | -0.734 | 0.051 | 2.086 | 0.049 |

As can be seen from the table, the model shows good fitting performance for the non-uniform distribution of the average annual settlement rate and cumulative settlement value in the study area. T-values and α values in the table indicate that the selected independent variables maintain their statistical significance within 95% confidence interval when predicting the annual average settlement rate and cumulative settlement value.

5.1.2 Independent Variable Analysis

Through the calculation of the three models, the distribution diagram of the influence coefficient of the independent variables corresponding to different models was obtained, as shown in Figure 6, 7 and 8.

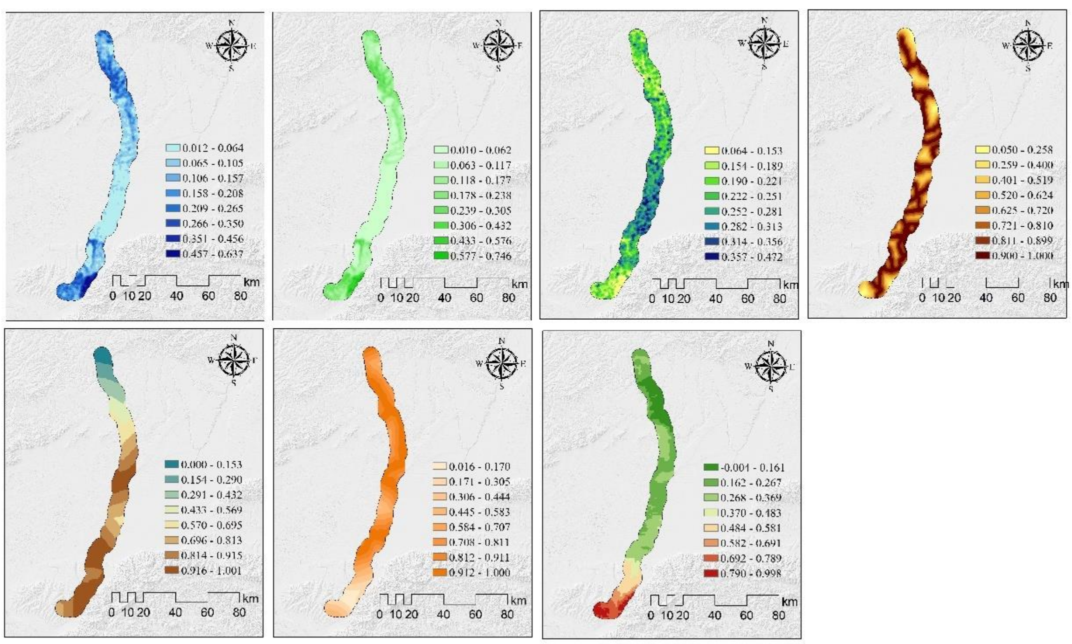

**Figure 6. The Results of the OLS Model**

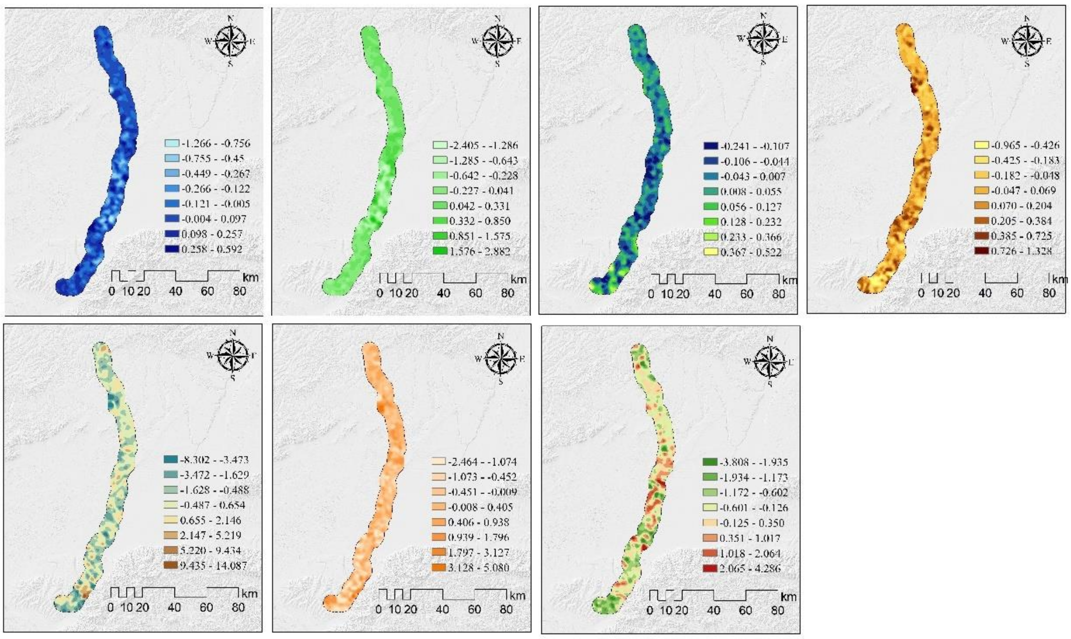


**Figure 7. The Results of the GWR Model**

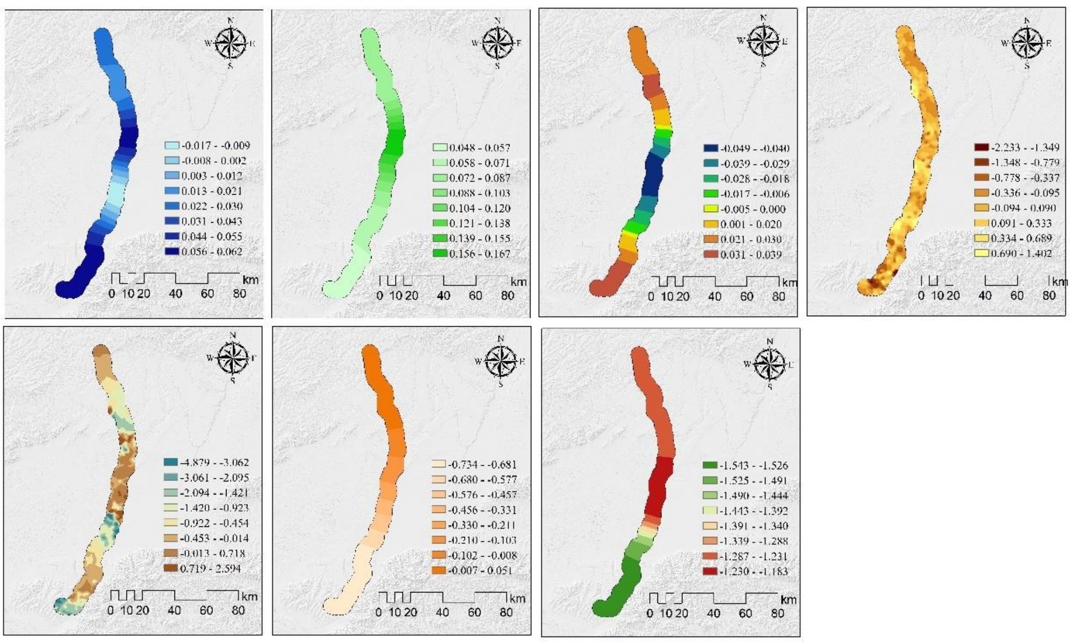


**Figure 8. The Results of the MGWR Model**

After statistical comparison of the results of the three models, it is found that the distance from the fault has the greatest impact on the land subsidence in the region, followed by the average annual rainfall. Due to the complex geological structure conditions in the study area, which is located in the Loess Plateau area and is dominated by loose thick layer loess, it is easy to slip through faults or collapse to the fracture zone. Moreover, rainfall is not evenly distributed throughout the year and is mainly concentrated in summer. Therefore, the distribution of faults plays a decisive role in the stability of loess region, and the distribution of rainfall plays a role in inducing settlement.

*5.2 Comparison of Model Results*

**Table 4. Comparison Table of Model Performance in the Study Area**

| Dependent variable | Average annual settling rate | | |
|---|---|---|---|
| Model | OLS | GWR | MGWR |
| Count | 8386 | 8386 | 8386 |
| $R^2$ | 0.084 | 0.702 | 0.726 |
| $AIC_c$ | -19174.5 | -26419.1 | 13907.9 |
| RSS | 48.799 | 12.924 | 2043.605 |
| Bandwidth | - | 84 | 44-3563 |

The MGWR model is compared with the traditional model, the higher the $R^2$, the better the fit; The lower the $AIC_c$ and RSS values, the higher the independent variable reproducibility level.

*5.3 Model Accuracy*

The calculation results of GWR model and MGWR model were used to draw the error prediction error map of space points in the study area. The area with small prediction error indicates that the prediction model has better adaptability in this area. As shown in Figure 9, both models have good adaptability in the region.

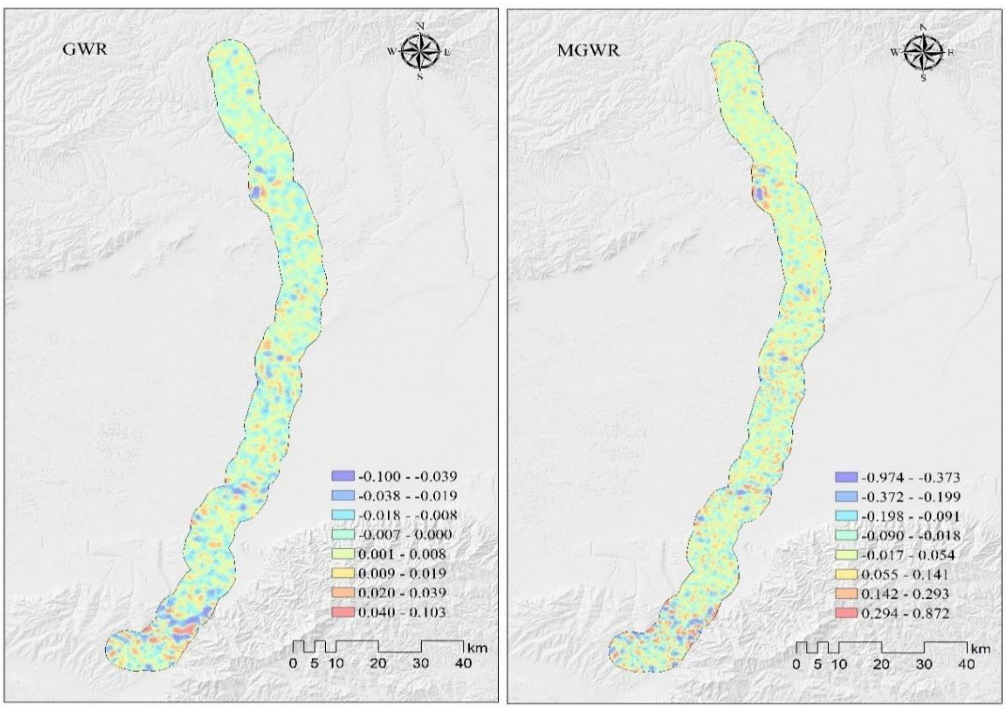


**Figure 9. Fitting Residual Distribution in the Study Area**

## 6. Conclusion and Discussion

According to the deformation characteristics in the 750kV third passage project area of northern Shaanxi and Guanzhong and its geological environment, 7 indexes including slope, topographic humidity index, distance from river, distance from road, distance from fault, rainfall and topographic relief were selected as independent variables, and the land subsidence was predicted by combining MGWR model and GIS technology. The following conclusions can be obtained:

(1) Based on the field investigation and InSAR results, this study used a spatial multi-scale geographical weighted regression model to predict the land subsidence along the 750kV third passage project in Shanbei and Guanzhong, Weinan City, Shaanxi Province. The model calculated the optimal bandwidth required by the simulation, and explored the spatial heterogeneity of different influencing factors. The influence of different factors in different regions of the route on land subsidence was quantitatively studied.

(2) As can be seen from the frequency distribution diagram of the spatial variation coefficient, among the seven independent variables selected, the fault distance, followed by precipitation, has a greater impact on the land settlement in the line region.

(3) From $R^2$ of the average annual deformation rate in the study area, it can be seen that MGWR model can better fit the land subsidence reflected by satellite monitoring data. Compared with GWR and OLS models, MGWR model has higher prediction accuracy, which is improved by 1000%. Moreover, this model can overcome the shortcomings that InSAR results cannot directly derive continuous and compact settlement field, and the prediction error is small, which can provide important reference value for the prevention and control of the ground subsidence disaster of the line.

## References

A.S. Fotheringham, W. Yang, & W. Kang. (2017). Multiscale geographically weighted regression (MGWR). *Ann. Am. Assoc. Geogr.*, *107*(2017), 1247-1265. https://doi.org/10.1080/24694452.2017.1352480

Daniel Yuh Chao. (2019). Weinan vegetation cover change and its correlation with climate factors. *Ecological science*, *42*(5), 92-103.

F. Raspini, F. Caleca, M. Del Soldato, D. Festa, P. Confuorto, & S. Bianchini. (2022). Review of satellite radar interferometry for subsidence analysis. *Earth Sci. Rev.*, *235*(2022), 104239. https://doi.org/10.1016/j.earscirev.2022.104239

Fadhillah, M.F., Achmad, A.R., & Lee, C. (2020). Integration of InSAR Time-Series Data and GIS to Assess Land Subsidence along Subway Lines in the Seoul Metropolitan Area, South Korea. *Remote Sens.*, *12*, 3505. https://doi.org/10.3390/rs12213505

Fan Shan-Shan, Guo Hai-Peng, Zhu Ju-Yan, et al. (2013). Linear regression model application in the prediction of land subsidence in Beijing. *Chinese journal of geological hazard and prevention and control*, *24*(01), 70-74.

Feng Xijie, & Dai Wangqiang. (2004). Lateral migration of fault activity in Weihe Basin. *Acta Seismologica Sinica*, *2004*(02), 174-182+230. https://doi.org/10.1007/BF02896933

H. Yu, A.S. Fotheringham, Z. Li, T. Oshan, W. Kang, & L.J. Wolf. (2020). Inference in multiscale geographically weighted regression. *Geogr. Anal.*, *52*(2020), 87-106. https://doi.org/10.1111/gean.12189

H. Yu, H. Gong, B. Chen, K. Liu, & M. Gao. (2020). Analysis of the influence of groundwater on land subsidence in Beijing based on the geographical weighted regression (GWR) model. *Sci. Total Environ.*, *738*(2020), 139405. https://doi.org/10.1016/j.scitotenv.2020.139405

He Hongqian. (2011). *Genetic mechanism of ground fractures in Weihe Basin*. Chang 'an University.

Hu, B., Zhou, J., Wang, J., Chen, Z., Wang, D., & Xu, S. (2009). Risk assessment of land subsidence at Tianjin coastal area in China. *Environ.Earth Sci.*, *59*, 269-276. https://doi.org/10.1007/s12665-009-0024-6

Huang Shuangfei. (2024). *Landslide based on multi-scale geographically weighted regression is used evaluation*. Central south university.

L. Zhang, Y. Li, & R. Li. (2023). Driving forces analysis of urban ground deformation using satellite monitoring and multiscale geographically weighted regression. *Measurement*, *214*(2023), 112778. https://doi.org/10.1016/j.measurement.2023.112778

Li Guangyu, Zhang Rui, Liu Guoxiang, et al. (2018). Sentinel-1A TS-DInSAR settlement monitoring and analysis in Beijing-Tianjin-Hebei region. *Journal of Remote Sensing*, *22*(04), 633-646.

Li Li. (2014). *Research on Land subsidence prediction model and its application*. Chang 'an University.

Li Xianggen, & Ran Yongkang. (1983). North slope of Huashan Mountain and front active fault of Weinan Yuan. *North China Seismological Science*, *1983*(02), 10-18+9.

Liu Hujun. (2004). *Formation and Evolution of Weihe Basin and uplift of East Qinling Mountains*. Northwest University.

P. Berardino, G. Fornaro, R. Lanari, & E. Sansosti. (2002). A new algorithm for surface deformation monitoring based on small baseline differential SAR interferograms. *IEEE Trans. Geosci. Remote Sens.*, *40*(2002), 2375-2383. https://doi.org/10.1109/TGRS.2002.803792

Peng Jianbing et al. (2012). *Ground fracture Disaster in Xi 'an*. Beijing: Science Press, 2012.

Peng Jianbing, Lu Quanzhong, Huang Qiangbing et al. (2017). *Ground fracture disaster in Fen-Wei Basin*. Beijing: Science Press.

Peng Jianbing, Su Shengrui, Mi Fengshou, et al. (1992). *Active faults and geological hazards in Weihe Basin*. Xi 'an: Northwest University Press.

Quan Xinchang. (2005). Study on fault structure in Weihe Basin. *Coal Geology of China*, *2005*(03), 1-4+8.

S. Ye, Y. Xue, J. Wu, X. Yan, & J. Yu. (2015). Progression and mitigation of land subsidence in China, *Hydrgeol. J.*, *24*(2015), 685-693. https://doi.org/10.1007/s10040-015-1356-9

Wang Zhiwang, Liao Yonglong, & Li Duanyou. (2006). Research on landslide risk regionalization based on logistic regression method. *Chinese Journal of Underground Space and Engineering*, *2006*(S2), 1451-1454.

Wang, J., Wang, C., Zhang, H., Tang, Y., Duan, W., & Dong, L. (2021). Freeze-Thaw Deformation Cycles and Temporal-Spatial Distributionof Permafrost along the Qinghai-Tibet Railway Using Multitrack InSAR Processing. *Remote Sens.-Basel.*, *13*, 4744. https://doi.org/10.3390/rs13234744

Wang, W., Wu, L., Gong, H., Fan, P., Wu, W., Zhou, Y., & Zhang, Z. (2019). Deformation Monitoring for High-Voltage Transmission Lines Using Sentinel-1A Data. *IOP Conf. Ser. Earth Environ. Sci.*, *252*, 32033. https://doi.org/10.1088/1755-1315/252/3/032033

Xie Huafei. (2011). *Research on Damage Assessment technology of Power grid caused by earthquake disaster*. Zhejiang University.

Xiong, Q. (2023). *Deformation monitoring and influencing factors analysis in coastal areas based on InSAR*. Donghua university of science and technology.

Yin Yueping, Zhang Zuochen, & Zhang Kaijun. (2005). Research on the status quo of land subsidence in China and its control measures. *Chinese Journal of Geological Hazards and Control*, *2005*(02), 1-8.

Yue-fei wang. (2023). *Weinan region ground fissure development characteristic and the liability evaluation*. Chang 'an university.

Zhang Maosheng, & Li Tonglu. (2011). Study on induced factors and formation mechanism of loess landslide. *Journal of Engineering Geology*, *19*(04), 530-540.

Zhang Puxuan. (2017). *Study on groundwater variation characteristics, monitoring and assessment in Guanzhong Plain, Shaanxi Province*. Xi 'an University of Technology.

Zhao Jingbo, & Chen Yun. (1994). Study on porosity and collapsibility of loess. *Journal of Engineering Geology*, *1994*(02), 76-83.

Zhao Wenwu, Fu Bojie, & Chen Liding. (2003). Northern shaanxi loess hilly-gully region terrain factors and the correlation analysis of soil and water loss. *Journal of soil and water conservation*, *2003*(3), 66-69.